This journal is © The Royal Society of Chemistry 2020

Supplemental Information

Two-dimensional metal-organic framework with perpendicular one dimensional nano-channel as precise polysulfides sieves for high efficient lithium−sulfur batteries

Zhi Chang,[1,2] Yu Qiao,[1] Jie Wang,[4] Han Deng,[1,2] and Haoshen Zhou[1,2,3*]

Affiliations:

[1]Energy Technology Research Institute, National Institute of Advanced Industrial Science and Technology (AIST), 1-1-1, Umezono, Tsukuba 305-8568, Japan.

[2]Graduate School of System and Information Engineering, University of Tsukuba,

1-1-1, Tennoudai, Tsukuba 305-8573, Japan.

[3]Center of Energy Storage Materials & Technology, College of Engineering and Applied Sciences, Jiangsu Key Laboratory of Artificial Functional Materials, National Laboratory of Solid State Micro-structures, and Collaborative Innovation Center of Advanced Micro-structures, Nanjing University, Nanjing 210093, P. R. China.

[4]International Center for Materials Nanoarchitectonics (WPI-MANA), National Institute for Materials Science (NIMS), Tsukuba, Ibaraki, Japan
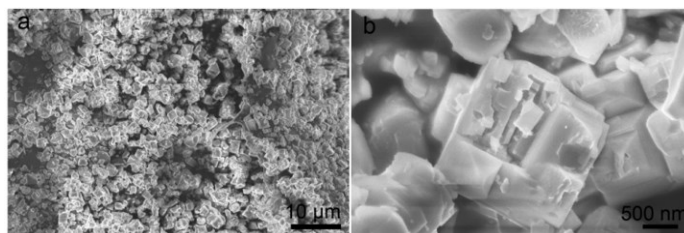
*Correspondence to: hs.zhou@aist.go.jp & hszhou@nju.edu.cn (H. Z.)
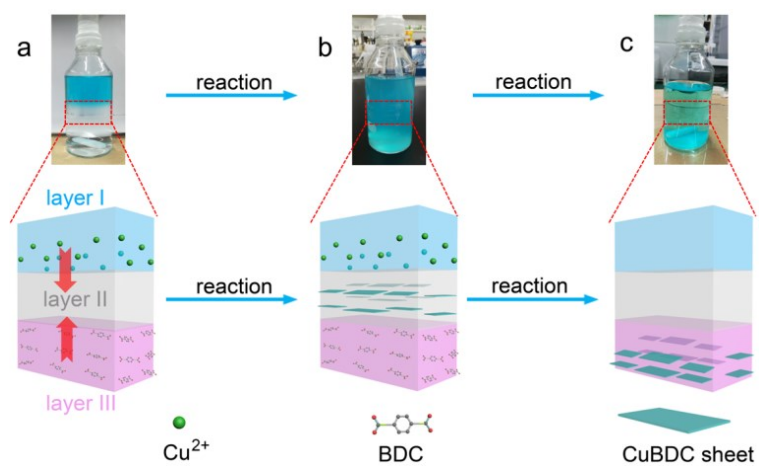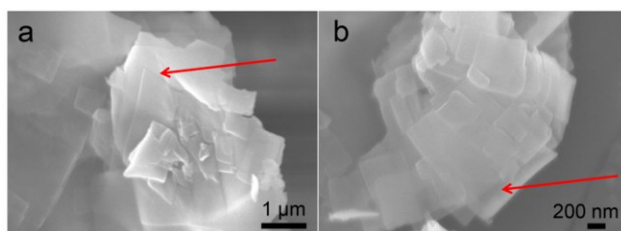
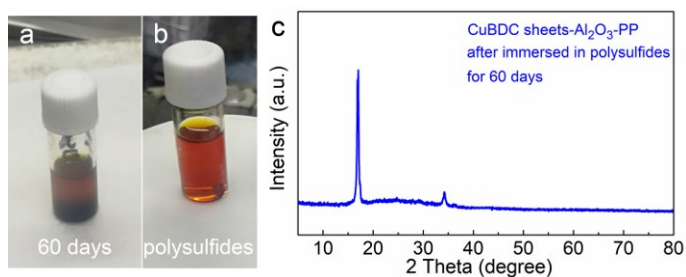**Figure S1.** Synthesis process of the obtained CuBDC nanosheets.

Figure S2. The CuBDC bulk solution prepared by using single solution method

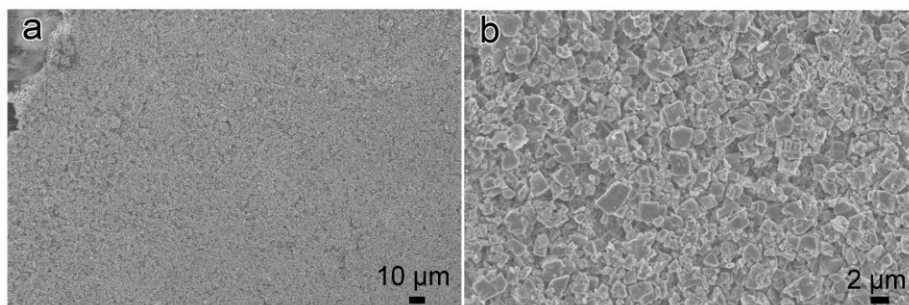**Figure S3.** SEM imaged of the obtained CuBDC bulk nanocomposites

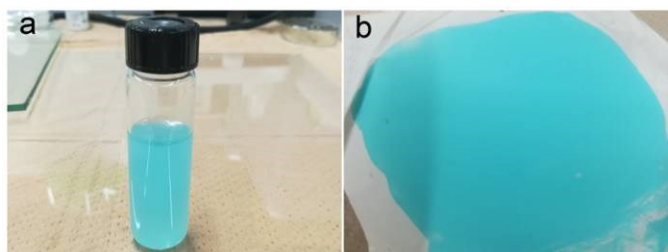**Figure S4.** SEM images of the obtained CuBDC nanosheets

Figure S5. The 2D CuBDC sheets powder immersed in polysulfides for more than 60 days and the corresponding XRD pattern of the 2D CuBDC sheets powder washed by DOL/DME after immersed in polysulfides for 60 days.
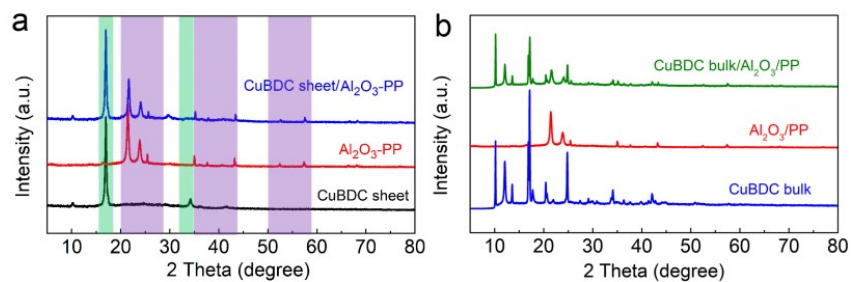
Figure S6. The digital photos of the CuBDC bulk coated Al$_2$O$_3$/PP separator.
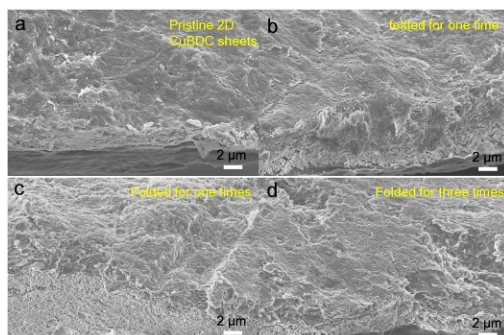

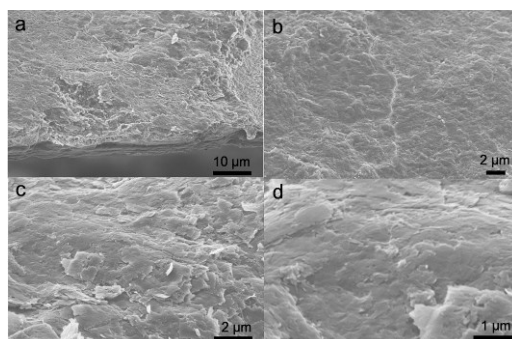**Figure S7.** SEM imaged of the obtained CuBDC bulk MOF separator

Figure S8. The photos of the obtained CuBDC nanosheets solution and the 2D CuBDC sheets coated separator.
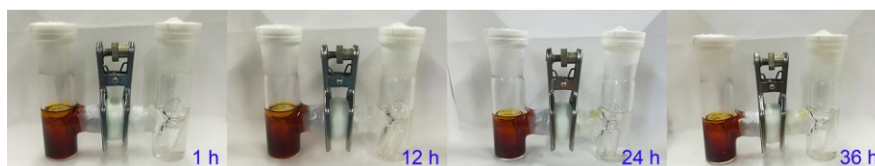
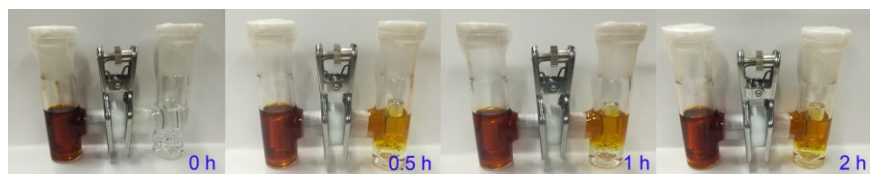**Figure S9.** XRD patterns of the two CuBDC MOF based separators

Figure S10. SEM images of the folded 2D CuBDC sheets separator.

Figure S11. SEM images of the pristine 2D CuBDC sheets separator before folded.

Figure S12. Polysulfides permission experiments of the CuBDC bulk based separator with the same mass loading as that of the 2D CuBDC sheets based separator.
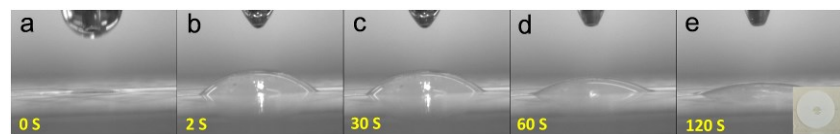
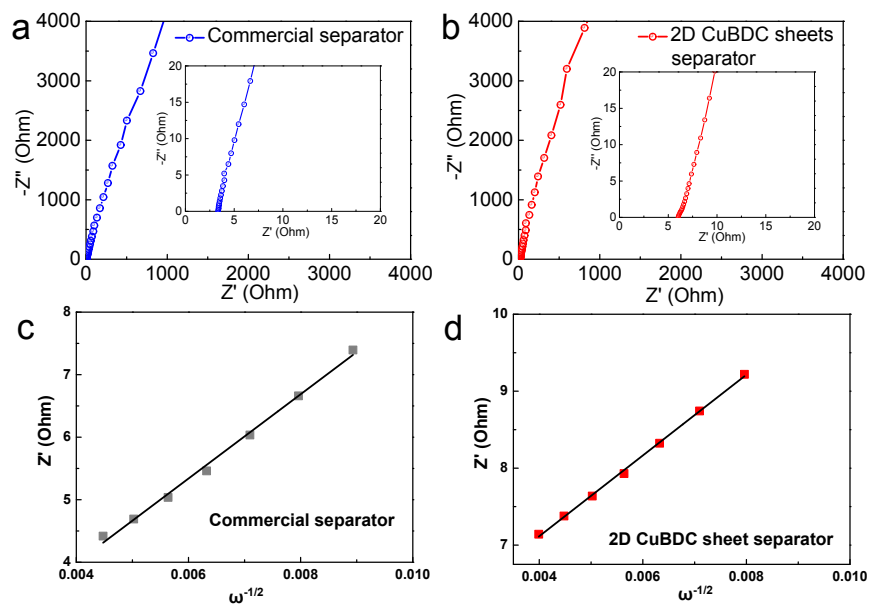**Figure S13.** Polysulfides permission experiments of the Al$_2$O$_3$/PP separator.
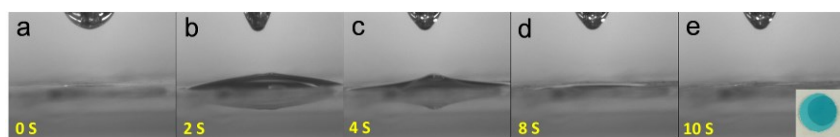
Figure S14. Wetting behavior LiTFSI/DOL-DME-based electrolyte on 2D CuBDC sheets separator.

Figure S15. Wetting behavior LiTFSI/DOL-DME-based electrolyte on PP separator.

Figure S16. Electrical impedance spectroscopy of (a) PP separator and (b) 2D CuBDC sheets separator and (c and d) the corresponding relationship between $\sigma\omega^{-1/2}$ and Z' of different separators.

The Li-ion diffusion coefficient (D_{Li}) of both the commercial separator and 2D CuBDC sheets based separator can be calculated from the formula shown in the following:

$$D = R^2T^2/2A^2n^4F^4C^2\sigma^2 \qquad (1)$$

Where D is ion diffusion coefficient, R is molar gas constant (8.314 J mol^{-1} K^{-1}), T is absolute temperature, A is electrode area, n is electron transfer number, and F is Faraday constant (96500 C mol^{-1}). C is the concentration of lithium ion. σ is Warburg factor, calculated by the formula:

$$Z' = R_\Omega + R_{ct} + \sigma\omega^{-1/2} \qquad (2)$$

(Z', R_Ω, R_{ct} and ω represent true resistance, Ohm solution impedance, charge transfer impedance and the frequency at low frequency region, respectively.) σ is the slope of the line $Z'\sim\sigma\omega^{-1/2}$ which can be obtained from the line of $Z'\sim\sigma\omega^{-1/2}$ (as Figure S16 c and d).

The calculated lithium diffusion coefficient D_{Li} (cm^2 s^{-1}) of the commercial separator is 5.75×10^{-12} cm^2 s^{-1}, however the lithium diffusion coefficient of 2D CuBDC sheets based separator is only 5.07×10^{-12} cm^2 s^{-1}. So, the lithium-ion diffusion coefficient of 2D CuBDC sheets based separator was only slightly lower than that of commercial separator.
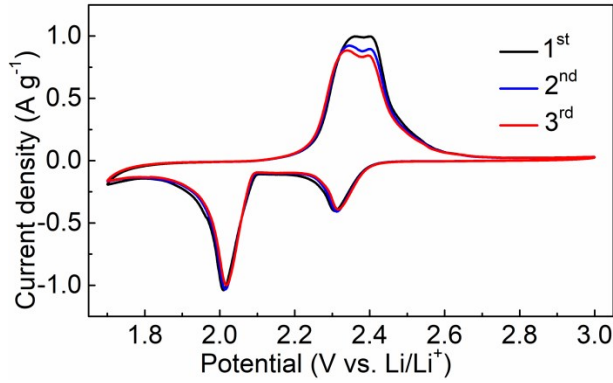
Figure S17. CV curves of the CuBDC bulk based Li−S battery.
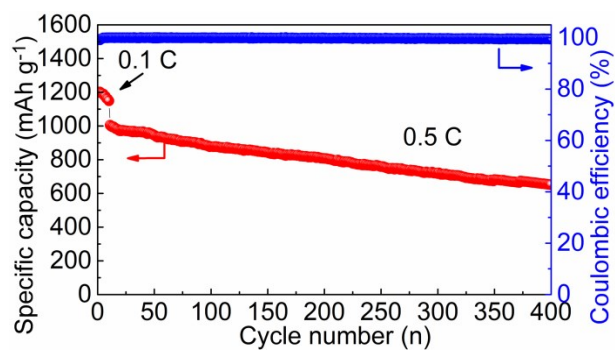
Figure S18. Cycling performance of the CuBDC bulk based separator Li−S battery at 0.5 C with the same MOF mass loading as that of CuBDC sheets based separator.
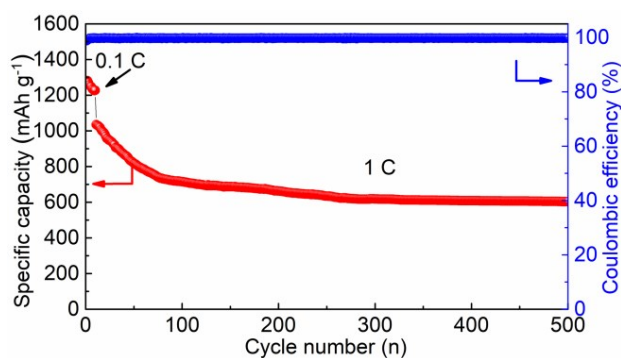
Figure S19. Cycling performance of the CuBDC bulk based separator Li−S battery at 1 C with the same MOF mass loading as that of CuBDC sheets based separator.
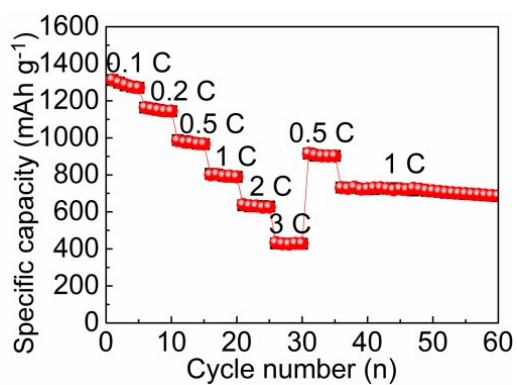
Figure S20. Rates performance of the CuBDC bulk based separator Li−S battery with the same MOF mass loading as that of CuBDC sheets based separator.

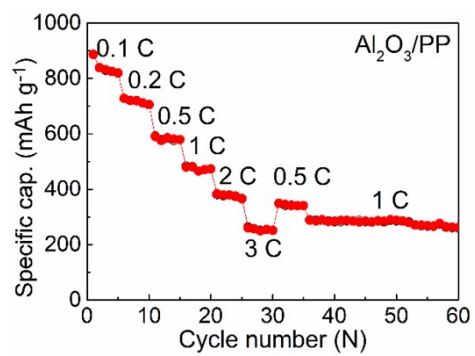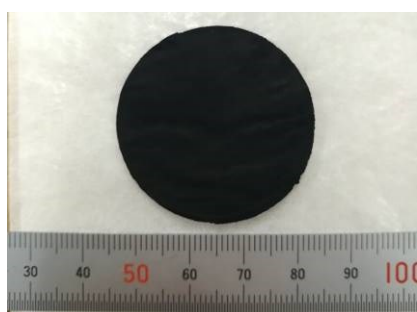**Figure S21.** Rates performance of the commercial separator Li−S battery.

Figure S22. Photos of the CNTs freestanding film before pounced into sulfur hosts.
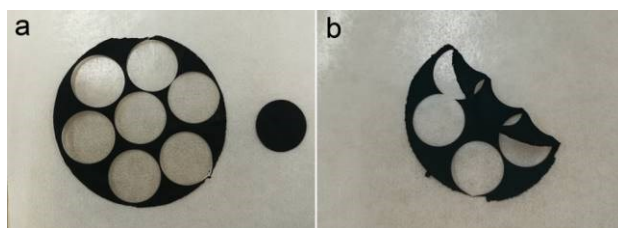
Figure S23. Photos of the CNTs freestanding film after pounced into sulfur hosts.
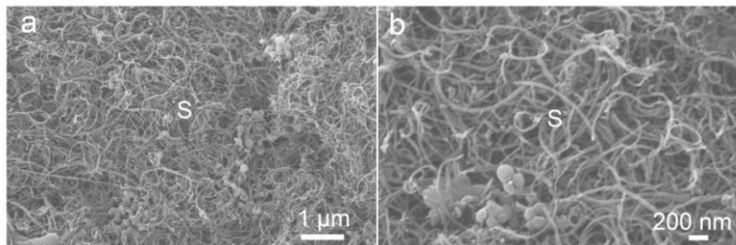
Figure S24. SEM images of the CNTs freestanding film after sulfur loading before heat treatment.
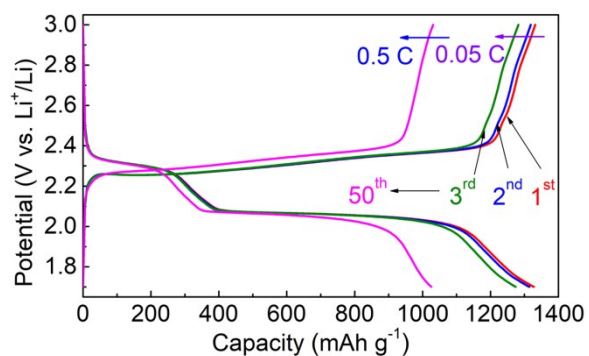
Figure S25. Electrochemical performances of the high sulfur loading (5.2 mg cm^{-2}) with MOF separator cycled at 0.5 C with initial activation at 0.05 C.
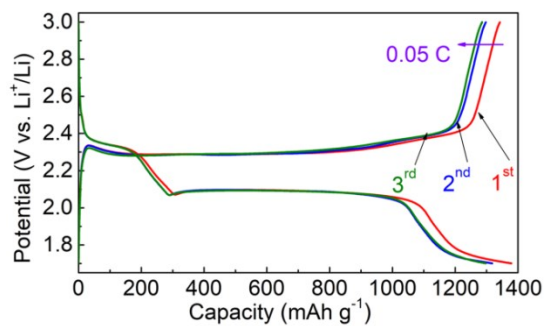
Figure S26. Electrochemical performances of the high sulfur loading of 4.6 mg cm^{-2} with MOF separator initially cycled at 0.05 C.
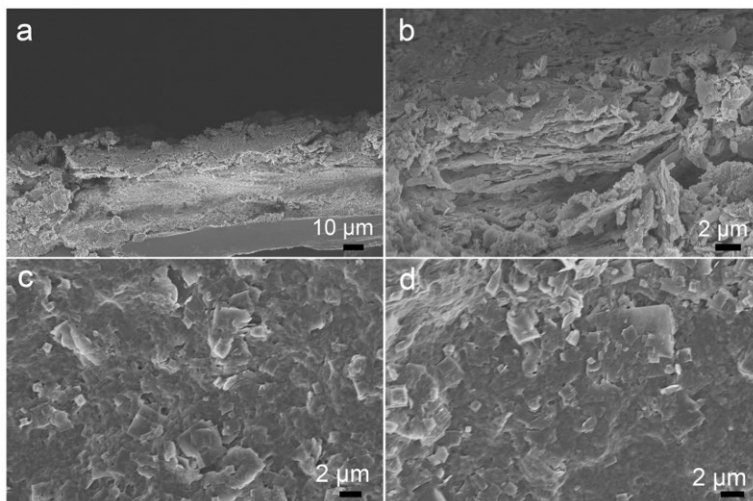
Figure S27. SEM images of the 2D CuBDC sheet based KJC/S cell after cycling for 500 cycles at 0.5 C.
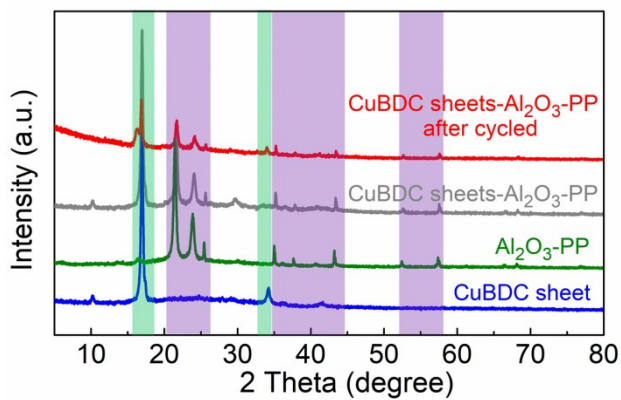
Figure S28. XRD pattern of the the 2D CuBDC sheet based KJC/S cell after cycling for 500 cycles at 0.5 C.
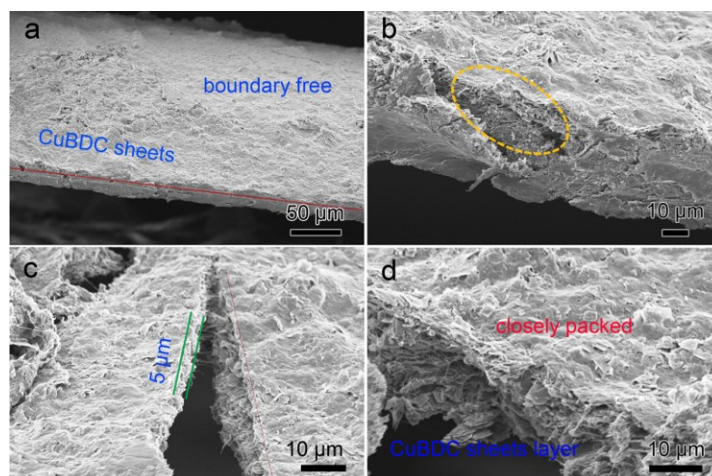
Figure S29. SEM images of the CuBDC sheet separator used in CNTs/S film based Li−S battery after cycled at 0.5 C for 500 cycles.
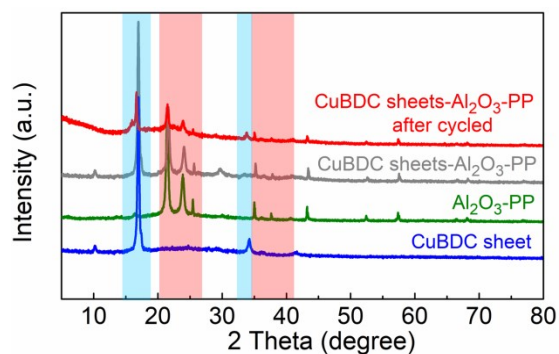
Figure S30. XRD pattern of the 2D CuBDC sheet based CNTs/S film cell after cycling for 500 cycles at 0.5 C.

Perfectly preserved 2D nanostructure can be suspected from the XRD pattern as highlighted by the light blue triangle. More important, no any peaks from sulfur species can be observed, which highlight the important role of CuBDC sheets in suppressing polysulfides.
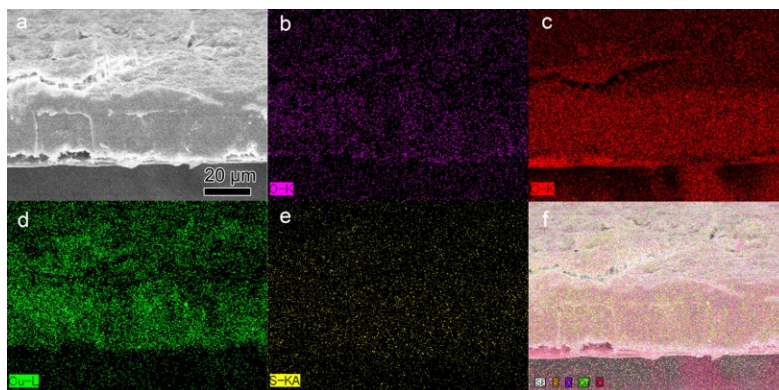
Figure S31. Elemental mapping of the CuBDC sheet separators after cycling.
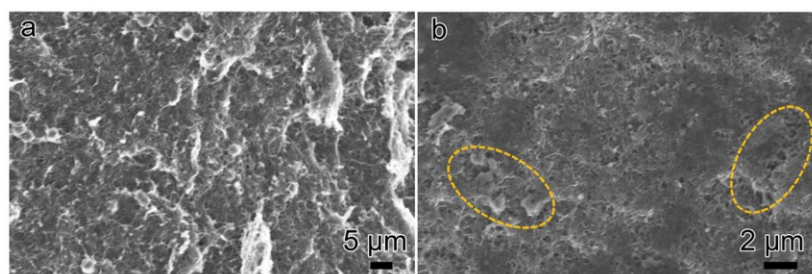
Figure S32. SEM images of the CNTs/S cathode after cycled at 0.5 C for 500 cycles.
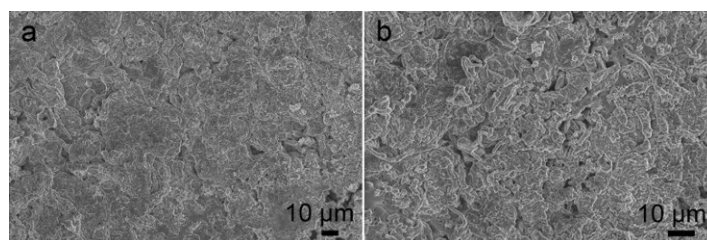
Figure S33. SEM images of the Li anodes from (a) 2D CuBDC sheets separator based Li−S battery with 5.2 mg cm^{-2} sulfur loading after cycled at 0.5 C for 500 cycles; (b) PP separator based Li−S battery with 2.2 mg cm^{-2} sulfur loading after cycled at 0.5 C for 500 cycles.

Table S1. Electrochemical performances of the Li−S batteries copped with multiple functional separators (with S loading below 2.0 mg cm^{-2})

Functional separators	S contents	S loading (mg cm^{-2})	Cycle life	Capacities (mAh g^{-1})	Capacity decay (per cycle)	Ref.
LDH/graphene	63%	1.1-1.3	1000	337 at 2 C	0.06%	S1
GO	35%	1.0-1.2	400	750 at 1 C	0.08%	S2
Meso-carbon	49%	1.55	500	591 at 2 C	0.06%	S3
Zn-MOF	70%	1.0	200	738 at 0.2 C	0.21%	S4
Graphite/LTO	90%	1.5	100	330 at 1 C	0.45%	S5
CNTs	70%	1.0	100	581 at 2 C	0.03%	S6
ZnBTC/GO	70%	0.6-0.8	350	685 at 3 C	0.09%	S7
Phosphorus	66%	1.5-2.0	100	800 at 1.2 C	0.07%	S8
2D CuBDC sheets	70%	1.8-2.3	**1000**	851 at 0.5 C	**0.04%**	This work
2D CuBDC sheets	70%	1.8-2.3	**400**	830 at 1 C	**0.02%**	This work

Table S2. Electrochemical performances of the Li−S batteries copped with multiple functional separators/interlayers (with high S loading about 3.5-6.0 mg cm^{-2})

Functional separators	S contents	S loading (mg cm^{-2})	Cycle life	Capacities (mAh g^{-1})	Capacity decay (per cycle)	Ref.
LDH/graphene	63%	4.3	100	800 at 0.2 C	0.06%	S1
Cellular graphene	80%	5.3	100	703 at 0.1 C	0.07%	S9
PP/GO/Nafion	60%	4	30	930 at 0.2 C	0.7%	S10
N-polymer/GO	70%	3.3	200	738 at 1 C	0.15%	S11
Porphyrin sheets	63%	3.6	400	688 at 0.2 C	0.16%	S12
MWCNT	53%	3.0	100	851 at 0.5 C	0.23%	S13
BaTiO$_3$	65%	3.0	50	925 at 0.1 C	0.34%	S14
2D CuBDC sheets	70%	5.2	**500**	795 at 0.5 C	**0.05%**	This work
2D CuBDC sheets	70%	4.6	**500**	516 at 1 C	**0.08%**	This work

References

[S1] H. J. Peng, Z. W. Zhang, J. Q. Huang, G. Zhang, J. Xie, W. T. Xu, J. L. Shi, X. Chen, X. B. Cheng, Q. Zhang, Adv. Mater. 2016, 28, 9551-9558.

[S2] M. Shaibani, A. Akbari, P. Sheath, C. D. Easton, P. C. Banerjee, K. Konstas, A. Fakhfouri, M. Barghamadi, M. M. Musameh, A. S. Best, ACS Nano 2016, 10, 7768-7779

[S3] J. Balach, T. Jaumann, M. Klose, S. Oswald, J. Eckert, L. Giebeler, J. Power Sources 2016, 303, 317-324

[S4] J.-K. Huang, M. Li, Y. Wan, S. Dey, M. Ostwal, D. Zhang, C.-W. Yang, C.-J. Su, U.-S. Jeng, J. Ming, ACS Nano 2018, 12, 836-843.

[S5] S. Niu, W. Lv, G. Zhou, H. Shi, X. Qin, C. Zheng, T. Zhou, C. Luo, Y. Deng, B. Li, Nano Energy 2016, 30, 138-145.

[S6] M. Li, W. Wahyudi, P. Kumar, F. Wu, X. Yang, H. Li, L.-J. Li, J. Ming, ACS Appl. Mater. Interfaces 2017, 9, 8047-8054.

[S7] S. Bai, K. Zhu, S. Wu, Y. Wang, J. Yi, M. Ishida, H. Zhou, J. Mater. Chem. A 2016, 4, 16812-16817.

[S8] J. Sun, Y. Sun, M. Pasta, G. Zhou, Y. Li, W. Liu, F. Xiong, Y. Cui, Adv. Mater. 2016, 28, 9797-9803.

[S9] H. J. Peng, D. W. Wang, J. Q. Huang, X. B. Cheng, Z. Yuan, F. Wei, Q. Zhang, Adv. Sci. 2016, 3, 1500268.

[S10] T. Z. Zhuang, J. Q. Huang, H. J. Peng, L. Y. He, X. B. Cheng, C. M. Chen, Q. Zhang, Small 2016, 12, 381-389.

[S11] C. Y. Chen, H. J. Peng, T. Z. Hou, P. Y. Zhai, B. Q. Li, C. Tang, W. Zhu, J. Q. Huang, Q. Zhang, Adv. Mater. 2017, 29, 1606802.

[S12] L. Kong, B. Q. Li, H. J. Peng, R. Zhang, J. Xie, J. Q. Huang, Q. Zhang, Adv. Energy Mater. 2018, 1800849.

[S13] H. M. Kim, J.-Y. Hwang, A. Manthiram, Y.-K. Sun, ACS Appl. Mater. Interfaces 2016, 8, 983-987.

[S14] T. Yim, S. H. Han, N. H. Park, M. S. Park, J. H. Lee, J. Shin, J. W. Choi, Y. Jung, Y. N. Jo, J. S. Yu, Adv. Funct. Mater 2016, 26, 7817-7823.